Tuning the Dynamics of Bistable Mechanisms by Introducing Travel Limits

Kylian van Puffelen, Thijs W. A. Blad(✉), and Ron van Ostayen

Department Precision and Microsystems Engineering,
Delft University of Technology, Delft, The Netherlands
t.w.a.blad@tudelft.nl

Abstract. Vibrations are a promising source for powering wireless sensors, for example in low-frequency environments like human motion. These environments suffer from unpredictable vibration spectra and their low-frequency and large amplitude characteristics offer great possibilities for mechanisms with double well potential energy characteristics. The dynamical output performance of a bistable mechanism depends on the oscillation in the large amplitude trajectory between the two potential wells. However, requires enough force to overcome potential energy barrier. This work aims to improve the occurrence of interwell oscillation by lowering the potential energy barrier between the two potential wells by the influence of hard mechanical travel limits. A bistable mechanism is numerically modelled and experimentally tested to investigate the influence of the mechanical travel limits for low-frequency excitations. An axial loaded buckling beam was used to introduce bistability and combined with a parallel guidance mechanism to compensate for the strong negative stiffness. A single-degree of freedom model is used to model the bistable characteristics and is expanded with a coefficient of restitution model to represent the mechanical characterization of the travel limits. This combination resulted in a decrease in required force for the oscillation in the desired large amplitude trajectory by constraining the oscillator motion with travel limits. Furthermore, the results from the numerical bistable model in combination with mechanical characteristics of the travel limits at impact, proves to be in good agreement with the experimentally obtained results.

Keywords: Vibration energy harvesting · Bistability · Low-frequency · Mechanical travel limits · Impact · Coefficient of restitution

1 Introduction

Buckled bistable oscillators are mechanisms, consisting of flexible elements and allow to travel with different trajectories between the stable equilibrium positions [1]. Their difference in comparison with conventional monostable mechanisms, are the potential energy characteristics. Monostable oscillators consist of a single potential energy well and are mostly designed to work as a resonant oscillator, resulting in high output performance on a specific frequency [2, 3]. However, if the oscillator is not accurately tuned to the input signal of the real world, poor output performance can be expected [4].

J. Beran et al. (Eds.): TMM 2020, MMS 85, pp. 134–143, 2022.
https://doi.org/10.1007/978-3-030-83594-1_14

The potential energy characteristics of bistable structures consist of double potential energy wells, which are segregated by an energy barrier. The barrier between the two wells allows the oscillator to travel with two distinct trajectories, intra- or interwell motion, respectively confined in one well, or between the wells [5]. The energy capture mechanism depends on the ability of the oscillator to move between the stable equilibria, however this oscillation can not always be guaranteed and depends on the height of the potential energy barrier. If the bistable oscillator is not designed properly, large amount of input energy is consumed to overcome the potential energy barrier. As a consequence, low range of motion as well as poor output performance can be expected, resulting in the requirement for high input acceleration signals [6].

In order to overcome this problem a positive stiffness can be used to counteract the strong negative stiffness of the bistable mechanism and reduces the height of the potential energy barrier. In the work of Blad et al. [7] the principle of static balancing is used to compensate for the negative stiffness. With this principle the potential energy barrier can be flattened, which reduces the energy consumption by the jump over the energy barrier. In the work of Zhu et al. [6] a midpoint magnetic force is added, to accomplish the same principle by actively tuning the height of the potential energy barrier with magnets.

However, both stiffness compensation mechanisms do not only reduce the potential energy barrier, but also reduces the advantage of the dynamical nonlinearities. Since the stiffness compensation counteracts the negative stiffness in the bistable mechanism, which is connected to the nonlinear snap-through motion [8]. In this work, a method is studied in which the travel limit is manipulated as a design parameter. This proposed design parameter reduces the height of the barrier by relocating the stable equilibrium positions in the mechanical domain with travel limits. This allows the oscillator to be tuned to the input excitation without having to compensate for the original stiffness characteristics between the stable equilibria positions.

In Sect. 2, the working principle and design of the bistable oscillator is presented, followed by a mechanical and dynamical analysis. Section 3 describes the results and are discussed in Sect. 4. The most significant conclusions are described in Sect. 5.

2 Method

2.1 Mechanical Design

The mechanical design and working principle of the planar bistable mechanism is shown in Fig. 1a–c. Figure 1a shows the mechanism after fabrication which consist of a shuttle suspended by two parallel flexures on one end, and a single flexure at the other end. In Fig. 1b the preloading process is shown, in which the initially flat mechanism is buckled by compressing it over a distance of *dl*. Figure 1c shows the post-buckled mechanism with the identified degree-of-freedom (DoF). In this mechanism, the boundary condition of the flexures are fixed.

The force-deflection relation of the motion in this DoF has the following interesting properties. The uncompressed monostable configuration in Fig. 1a, consist only of positive stiffness and has a straight line relation as force-deflection characteristics. As soon as bistability is introduced, the single flexure is buckled and the mechanism consist of two stable equilibrium positions, as can be seen in Fig. 1b. Between the stable equilibria

the positive stiffness is altered with a negative stiffness slope and exhibits nonlinear phenomena. The mechanism losses stability as it acquire enough input force, this will result in an attractive force to the other stable equilibria position, and is called snap-through motion. This nonlinearity improves the ability of bistable oscillators to outperform their performance in comparison with monostable oscillators [9].

From theory, we know that this mechanism will deflect as it acquire enough force [10]. In this work, it is expected that the force required for action is influenced by hard mechanical travel limits as can be seen fin Fig. 1c. Because of this limitation, the motion of this DoF is reduced and the system will come at rest at an other stable equilibrium position. This position is much closer to the local maximum of the potential energy curve and therefore requires less input force for interwell motion. To investigate this phenomena a contactless force will be exerted on the mechanism with the use of a mass and an acceleration signal, to examine the influence of the travel limits on the required force for interwell motion. Moreover, the dependency of the stable equilibria positions is uncoupled from the preload by the integration of the new design parameter. In this configuration the height of the potential energy barrier can be set with the preload and influenced with the design parameter by relocating the stable equilibrium positions.

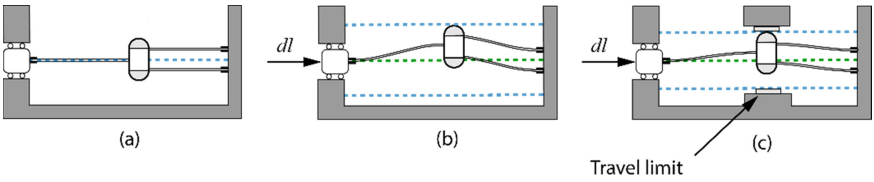

Fig. 1. Schematic working principle of the bistable mechanism, in blue stable and in green unstable equilibrium positions. a.) Monostable structure, b.) Unconstrained bistable structure, c.) Constrained bistable structure with travel limits

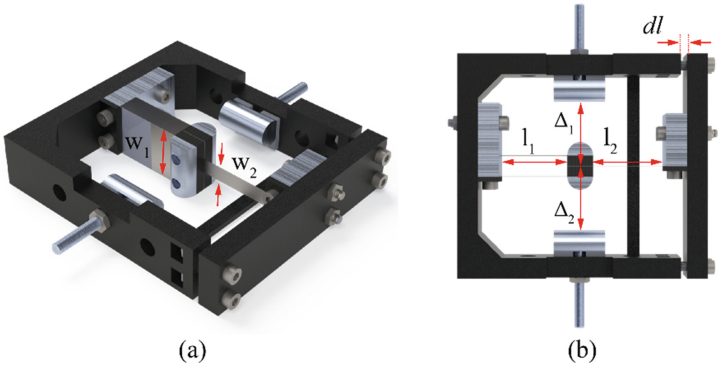

Fig. 2. The unloaded planar bistable mechanism design with indicated parameters, a) Isometric view, b) top view

2.2 Fabrication

The bistable mechanism prototype can be seen in Fig. 2. The flexural beams in this design are made from 0.1 mm thick spring steel with the properties: ($E_f = 190$ GPa, $v_f = 0.34$ $\rho_f = 7.89\ \frac{kg}{m^3}$) and are manufactured using a micro laser cutting machine. The proofmass was constructed out of a stack of steel shims and squeezed by two cylindrical shaped aluminium components with the following properties: ($E_s = 69$ GPa, $v_s = 0.34$, $\rho_s = 2.70\ \frac{kg}{m^3}$). The same shape of the aluminium components were used for the travel limits, however placed perpendicular to the orientation of the proofmass to create a Hertz contact point. Both cylinders of the proofmass and travel limits have corresponding dimensions for the radius (5 mm) and length (20 mm). The frame was 3D printed in PLA at 100% infill, in order to give the system its maximum rigidity and hinder the influence of its flexibility during dynamical loading.

An important design aspect in bistable mechanisms are the clamping conditions of the suspensension, slight differences in alignment tightening torque and material stiffness, result in different behaviour. Therefore the assembly procedure was according to the following order. A spacer with thickness *dl* were used to fill the gap between the main frame and the tightening bracket, then the bistable suspension were installed in the unloaded configuration as shown in Fig. 1a. As the suspension was installed, the spacer was removed and the bracket was tightened. In this order, the bistability could be introduced and guaranteed with the correct predefined axial load displacement. The tuning parameter in this design is defined in Fig. 2 with the travel limit (Δ), which defines the locations of the new stable equilibria positions. The variation of this parameter is done with the use of 0.5 mm thick spacers and placed between the frame and the backside of the travel limits, which were kept in place with a screw thread. Furthermore, the parameters used for this prototype are summarized in Table 1.

Table 1. Planar bistable mechanism design parameters

Parameter	Symbol	Value
Unloaded parallel flexure length	l_1	26 mm
Unloaded buckling flexure length	l_2	27.7 mm
Parallel flexure width	w_1	20 mm
Buckling flexure width	w_2	6.8 mm
Axial displacement	*dl*	2.7 mm
Proofmass weight	m	0.0152 kg

2.3 Numerical Model

Finite Element Analysis

To model the dynamical performance, the force-deflection relation of the motion in the DoF in this bistable mechanism was obtained first. This mechanical analysis was

performed in a finite element (FEM) analysis in ANSYS Mechanical APDL. The model was constructed out of BEAM 188 elements based upon Timoshenko's beam theory. To model the bistable characteristics, both ends of the structure were constrained and the in plane longitudinal degree-of-freedom of the single buckling flexure were relieved. On this flexure, a small force was applied in the middle, to help the system to bifurcate to the first buckling mode when an axial load displacement (*dl*) was applied on the relieved DoF. After the bistability was introduced, a displacement were applied on the middle of the proofmass, where simultaneous the reaction forces were recorded. The simulated force deflection behaviour can be obtained in Fig. 3.

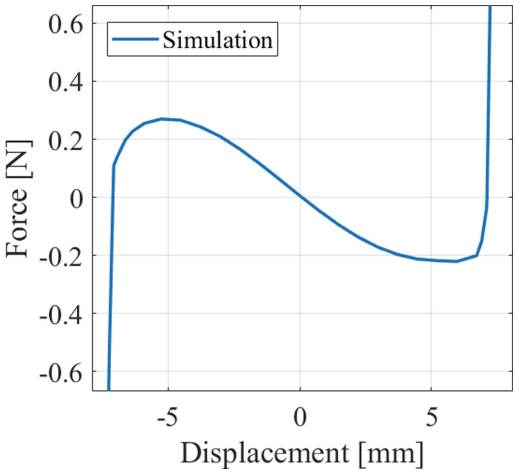

Fig. 3. Simulated force-deflection behaviour of the bistable mechanism

Dynamical Analysis

The dynamical model of the bistable system is described using a lumped-parameter single-degree-of freedom model. Without the interaction of the travel limits, the system can be described using the mass-spring-damper model, represented by equation Eq. (1):

$$m\ddot{x} + c\dot{x} + F_{Mechanism}(x) = F(x) \tag{1}$$

In this equations x, $\dot{x}$ and $\ddot{x}$ represent the oscillator displacement, velocity and acceleration relative to its base excitations. The mass (m) of the system is defined by the weight of the proofmass and damping coefficient (c) is calculated with the observed damping ratio ($\xi = 0.023$) during a logarithmic decrement measurement, where the system at rest is excited with an plucking based motion. The nonlinear force of the bistable oscillator suspension is defined as $F_{Mechanism}$ and is extracted locally from the force-deflection simulation. The locations of the stable equilibria of the unconstrained configuration are defined by the amount of pretension, however the introduction of mechanical travel limits results in an expansion of the equation of motion with an extra nonlinear force. This force is defined as the parameter, responsible for the new locations of the stable equilibria, when the motion is constrained by the mechanical travel limits as can be observed from Fig. 1c.

When the stable equilibria are shifted, the stiffness and damping of the system increases significantly due to the rigid characteristics of the travel limits. The contact mechanics of this additional force of the travel limits is simplified using a coefficient of restitution (CoR) model, where the incoming velocity is reduced with an reduction factor of CoR = 0.36. This value represent the amount of kinetic energy loss at the collision with the travel limit. This value was observed during impact measurement, where the prototype was excited with a sinusoidal input excitation and the bouncing behavior of the impact were recorded with an laser sensor. The expression of Eq. (2) is used in the model [11].

$$CoR = \frac{V2}{V1} \tag{2}$$

The synthesis of the models are integrated as follows: the lumped-parameter model is calculated using the ODE solver in MATLAB. As soon as the oscillator reaches the travel limit, a collision is detected by an Event function in the ODE solver and changes the direction and reduces the incoming velocity according to the relation of Eq. (2). This procedure is repeated until all the energy is dissipated by the travel limit. The point of interest is the point at which the system loses stability and deflects between the stable equilibria positions, therefore an acceleration input signal is used to excite the model and repeated for varies travel limit positions. To represent an linear increasing acceleration sweep, a time series of 10 s is used for each separate acceleration signals between 0 g and 2 g, with an incremental increase of 0.02 g. From each signal the RMS velocity was calculated when the oscillator reached steady state conditions.

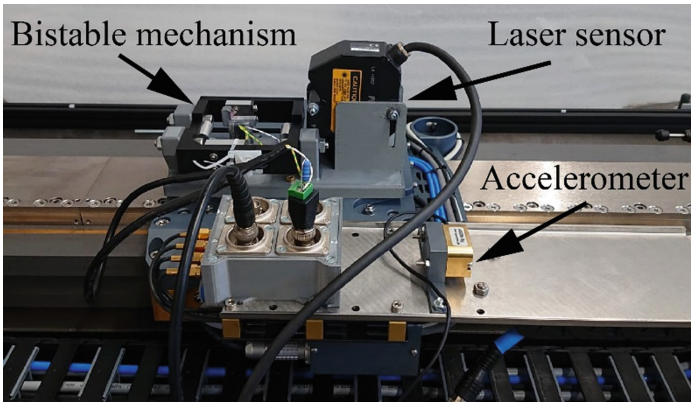

Fig. 4. Overview of the experimental setup on the linear air bearing stage

2.4 Experimental Characterization

Experimental Setup. The validation of this numerical model is performed on a custom made linear air bearing stage, shown in Fig. 4. This stage consist of a range of motion of 500 mm and is able to perform experiments for low frequency and large amplitude excitations. A DaQ chassis consisting of a NI-9215 and NI-9263 module were used. The

NI-9263 output module were used to provide the controller with input signals to actuate the air bearing stage. Although the controller is feedback controlled, an external AS28e 5g accelerometer is used to check the consistency of the input/output relation of the stage. A Keyence LK-H052 laser sensor were used to record the dynamical performance of the bistable mechanism. By placing the laser sensor on top of the base, relative displacement of the proofmass with respect to the base excitation could be recorded and simultaneously measured with the acceleration data by the NI-9215 input module.

Experimental Measurement. In order to rely on the numerical outcomes of the simulation, the dynamical performance is experimentally tested to validate the correctness. The measurement were executed as follows. The bistable mechanism is excited with a sinusoidal acceleration sweep, in order to provide a contactless force and investigate the influence of the travel limits on the acquired force to deflect between the stable positions. The sweep is started from rest with zero initial conditions and swept linearly from 0 g to 2 g acceleration over a time span of 300 s to ensure that each acceleration signal reaches steady state conditions. The excitation were kept at a constant frequency of 3 Hz. During this measurement, the displacement of the proofmass and the acceleration profile of the base excitation were measured and used as a check for correctness of the numerical model.

3 Results

In Fig. 6 the calculated oscillator travel results from the numerical model are compared with the experimentally obtained results. From this figure it can be seen that both results yield towards the same deflection point, where the contactless force from the acceleration profile is enough to overcome the potential barrier and start to bifurcate from intrawell to steady state interwell oscillation. From the section view, minor differences are observable in the rebounce when the travel limits are triggered.

In Fig. 6. the numerical calculated RMS velocity results for different accelerations and travel limit distances are shown. From the diagonal line in the surf plot, it can identified that less force is required for oscillation in the desired interwell trajectory as the bistable oscillator motion is more constrained by the travel limits.

4 Discussion

The dynamical response of the numerical model and the experimentally investigated response of the prototype, observed in Fig. 5, yield both towards the same deflection point as the acceleration sweep is linearly increased for a frequency of 3 Hz. Though difference could be observed at the impact as can be seen in the section view. The rebounce of the experiment consist of a maximum error of 8%, which means a small inaccuracy and result in larger damping characteristics than experimentally measured. However, from this figure it can also be seen that the rebounce characteristics of the experiment is not the same in both stable equilibrium positions, the reason can be explained by the small errors

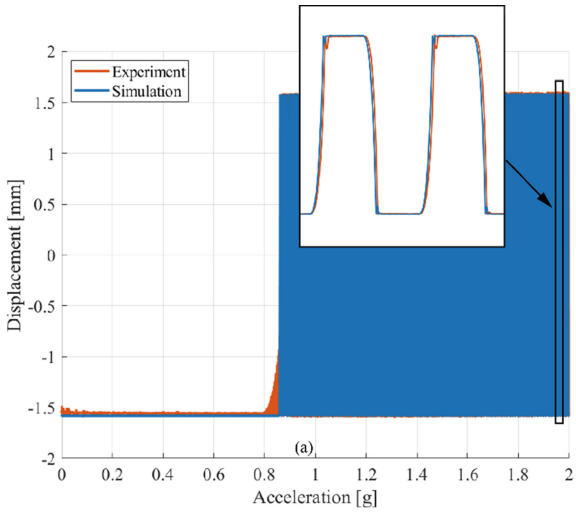

Fig. 5. Experimental validation of simulated dynamical response of an acceleration sweep and frequency of 3 Hz

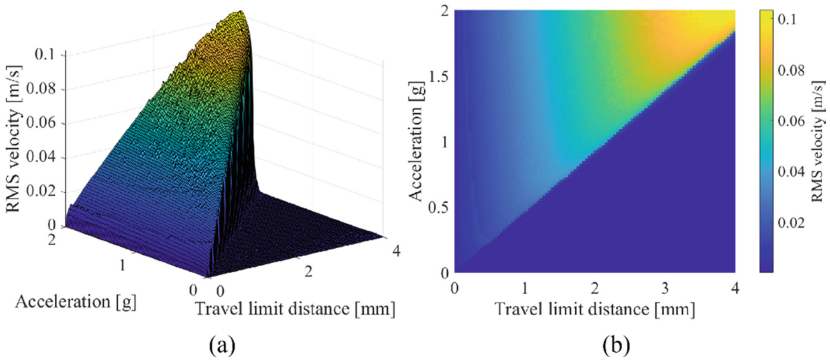

Fig. 6. Numerical calculated RMS velocity results for different accelerations and travel limit distances, a) Isometric view, b) Top view of the surf plot

in the location of the travel limits in the prototype, which causes this small asymmetrical behaviour of the rebounce at the collision in the experiment.

The surf plot of Fig. 6. confirms the research objective, from this plot it can be observed that less input force for actuation is needed for interwell oscillation as the motion is more constrained. However, this does not directly mean that constraining the oscillator motion will result in a better dynamical performance, but depends on a trade-off between maximum allowable decrease in RMS velocity and required force for actuation. In other words, as oscillation occur at for example an acceleration signal of 1g and the travel limit distance is set to 4 mm, the bistable oscillator has the freedom to oscillate, but the input force is too low and poor dynamical performance can be expected. The method described in this paper recommends to tune the travel limit distance, however in case

of excessive tuning by constraining the motion too much, it has the ability to oscillate but not the freedom to move due to the travel limits. Therefore a trade-of should be made first and the travel limit distance should be found with an optimisation process to estimate for each different environment the correct location for the travel limit distance.

5 Conclusion

In this work, the use of travel limits was studied as a method to reduce the energy barrier of bistable mechanisms such that interwell motion can be more easily achieved. The bistable mechanism was constructed from a flexure that was fixed at both ends and compressed beyond the point of buckling. A proofmass was mounted in the middle of the flexure and its motion is constrained by a mechanical stop. A numerical model was constructed to study the dynamics of this mechanism in which the travel limit is manipulated as a design parameter. The force-deflection relation of the bistable mechanism was obtained through finite element simulation and used as an input for the dynamical model. It was demonstrated that tuning the travel limit can result in an increased RMS velocity of the proofmass by allowing interwell motion. A prototype was constructed and tested experimentally under low-frequency vibrations to validate the results. It was found that travel limits can be used as a method to achieve interwell motion in bistable systems. It is recommended for future work to expand this research on bistable mechanisms by incorporating a transducer and comparing the performance for energy harvesting applications.

References

1. Masana, R., Daqaq, M.F.: Relative performance of a vibratory energy harvester in mono- and bi-stable potentials. J. Sound Vib. **330**(24), 6036–6052 (2011). https://doi.org/10.1016/j.jsv.2011.07.031
2. Blad, T.W.A., Tolou, N.: On the efficiency of energy harvesters: a classification of dynamics in miniaturized generators under low-frequency excitation. J. Intell. Mater. Syst. Struct. **30**(16), 2436–2446 (2019). https://doi.org/10.1177/1045389X19862621
3. Zhu, D., Harris, N., Beeby, S.: Performance of linear vibration energy harvesters under broad-band vibrations with multiple frequency peaks. Procedia Eng. **47**, 5–8 (2012). https://doi.org/10.1016/j.proeng.2012.09.070
4. Blystad, L.-C.J., Halvorsen, E.: A piezoelectric energy harvester with a mechanical end stop on one side. Microsyst. Technol. **17**(4), 505–511 (2011). https://doi.org/10.1007/s00542-010-1163-0
5. Harne, R.L., Wang, K.W.: A review of the recent research on vibration energy harvesting via bistable systems. Smart Mater. Struct. **22**(2), 023001 (2013). https://doi.org/10.1088/0964-1726/22/2/023001
6. Zhu, Y., Zu, J.W.: Enhanced buckled-beam piezoelectric energy harvesting using midpoint magnetic force. Appl. Phys. Lett. **103**(4), 041905 (2013). https://doi.org/10.1063/1.4816518
7. Blad, T.W.A., van Ostayen, R.A.J., Tolou, N.: A method for tuning the stiffness of building blocks for statically balanced compliant ortho-planar mechanisms. Mech. Mach. Theory **162**, 104333 (2021). https://doi.org/10.1016/j.mechmachtheory.2021.104333

8. Ha, C.S., Lakes, R.S., Plesha, M.E.: Design, fabrication, and analysis of lattice exhibiting energy absorption via snap-through behavior. Mater. Des. **141**, 426–437 (2018). https://doi.org/10.1016/j.matdes.2017.12.050
9. Jiang, W.-A., Chen, L.-Q.: Snap-through piezoelectric energy harvesting. J. Sound Vib. **333**(18), 4314–4325 (2014). https://doi.org/10.1016/j.jsv.2014.04.035
10. Jia, Y.: Review of nonlinear vibration energy harvesting: duffing, bistability, parametric, stochastic and others. J. Intell. Mater. Syst. Struct. **31**(7), 921–944 (2020). https://doi.org/10.1177/1045389X20905989
11. Ashraf, K., Md Khir, M.H., Dennis, J.O., Baharudin, Z.: A wideband, frequency up-converting bounded vibration energy harvester for a low-frequency environment. Smart Mater. Struct. **22**(2), 025018 (2013). https://doi.org/10.1088/0964-1726/22/2/025018